Ceramics International 43 (2017) 11992–11997

Contents lists available at ScienceDirect

Ceramics International

journal homepage: www.elsevier.com/locate/ceramint

Film thickness effect on texture and residual stress sign transition in sputtered TiN thin films

Yeting Xi[a], Kewei Gao[a], Xiaolu Pang[a,*], Huisheng Yang[a], Xiaotao Xiong[b], Hong Li[b], Alex A. Volinsky[c]

[a] School of Materials Science and Engineering, University of Science and Technology Beijing, Beijing 100083, China
[b] Institute for Advanced Materials and Technology, University of Science and Technology Beijing, Beijing 100083, China
[c] Department of Mechanical Engineering, University of South Florida, Tampa, FL 33620, USA

ARTICLE INFO

Keywords:
Ceramic films
GIXRD
Texture
Residual stress
Compressive-to-tensile transition
Mechanism

ABSTRACT

Residual stress in thin films and coatings strongly affects their properties and behavior in service. Comprehensive understanding and precise measurements of residual stress are prerequisites for preparing high quality films and coatings. Residual stresses in TiN films with different thickness were measured by X-ray diffraction (XRD) employing the $\cos^2\alpha \sin^2\psi$ method with certain optimization. Grazing incidence parallel beam optics was combined with side-inclination geometry using in-house designed sample stage to ensure results accuracy. To validate this method, TiN films with thickness ranging from 1 to 3 μm were deposited on (100) Si single crystal substrates at 300 °C by RF magnetron sputtering. High compressive −2 GPa residual stress was present in the 0.9 μm thick film and decreased with film thickness. Tensile stress of less than 0.3 GPa was present in 2 μm TiN film. Compressive-to-tensile residual stress transition was observed with the film thickness increase. Microstructure change with growth, annihilation of grain boudaries, atomic peening and recovery mechanisms are responsible for the reported stress sign transition.

1. Introduction

Brittle ceramic thin films and coatings of transition metal nitrides have many different applications in various devices because of their excellent properties [1,2]. As a protective layer, they must remain intact during service to ensure device reliability [3]. Residual stress is one of the most important factors contributing to device reliability. Mechanical properties of deposited films, including hardness, adhesion, fracture toughness and tribological properties are strongly affected by the residual stress [2–4]. Consequently, residual stress can lead to various film failures, including cracking, buckling and delamination [5–8]. Recent study indicates that the brittle film fracture could induce cracking of the ductile substrate and cause its premature failure at relatively low strain levels, rather than protecting the substrate [9].

The overall film residual stress is affected by thermally induced stress, stress resulting from film growth, externally applied and environmental stresses [10]. X-ray diffraction (XRD) and substrate curvature methods are the most commonly used techniques to characterize residual stresses in thin films or coatings [11]. Several research studies have focused on film thickness effects on residual stress. Most studies utilized the substrate curvature method [12,13]. Machunze et al. investigated residual stress in magnetron sputtered TiN thin films with thickness ranging from 0.02 to 1.9 μm on silicon substrates. From the substrate curvature measurements, it was found that the average film stress was compressive in all samples. Higher compressive average residual stress was present in thinner films and the stress decreased with the film thickness [3,14]. Köstenbauer et al. measured residual stress in 0.3–2.9 μm thick TiN films and provided a relationship between the film thickness and stress [15]. Compressive film stress decreased from −2.7 to −1 GPa with the film thickness. Other studies employed XRD methods to characterize residual stress in thin films [16,17]. Wang et al. measured compressive residual stress of −3.04, −2.4 and −1.98 GPa in 1.55, 2.69 and 3.89 μm thick TiN films using the modified XRD method [18]. Additionally, Daniel et al. deposited CrN films from 0.1 to 3 μm by reactive magnetron sputtering. Both substrate curvature and XRD $\sin^2\psi$ stress measurement techniques were used. CrN layer with 100 nm thickness exhibited the maximum compressive stress of −2.1 GPa, which rapidly decreased to −1.2 GPa with the film thickness increasing up to 500 nm. Thicker 1–3 μm CrN films had almost the same residual stress approaching −1 GPa [19]. Chou et al. reported residual stress variation measured by the $\sin^2\psi$

* Corresponding author.
E-mail addresses: pangxl@mater.ustb.edu.cn (X. Pang), volinsky@usf.edu (A.A. Volinsky).

http://dx.doi.org/10.1016/j.ceramint.2017.06.050
Received 24 April 2017; Received in revised form 1 June 2017; Accepted 7 June 2017
Available online 08 June 2017

XRD method with the TiN film thickness varied from 0.22 to 1.68 μm (0.22, 0.32, 0.75, 1.24 and 1.68 μm). Residual stress in the films ranged from −5.93 to −2.7 GPa with increased film thickness [20]. Chang et al. deposited TiAlN/CrN multi-layered 4 μm thick coatings and measured residual stress by X-ray diffraction. They found that the residual stress of all as-deposited films was compressive and varied from −3.9 to −6.2 GPa [21]. Karlsson investigated residual stress and mechanical properties of TiC_xN_{1-x} thin films with x = 0, 0.15 and 0.45. Initial compressive stress in all films was about −5.4 GPa. The film thickness was 3.2, 3.5 and 3.8 μm, respectively [22]. Residual stress in brittle films of similar materials systems shows great variation measured by different methods [23–26].

When brittle film thickness reaches a critical value, it can crack and/or peel from the substrate [27,28]. This critical thickness depends on both the film-substrate system and specific deposition conditions [29]. Film cracking or peeling can be driven by the residual stress, and tensile stress is more likely to cause film fracture [24,30–33]. From previous work, the reported residual stress is compressive in most ceramic thin films. In this study, compressive-to-tensile residual stress transition was found with increasing thickness of sputtered TiN thin films on Si substrates. This is similar with the results obtained by the substrate curvature method [34]. However, the curvature method has its own limitations and shortcomings. The curvature method is based on substrate profile measurements before and after film deposition using a profilometer. Two separate measurements before and after film deposition cause lower accuracy and repeatability. Also, curvature methods provide average macroscopic, rather than localized residual stress.

Microscopic d-spacing of crystallographic planes is measured in XRD methods [25]. Crystallographic planes spacing change is caused by the residual stress and is reflected by the diffraction reflections shift. Measuring the lattice parameter change is the basic idea of residual stresse measurements using XRD. Typical accuracy of the lattice parameter measurement is at least 0.001 Å, corresponding to 0.024% variation for an average TiN lattice parameter of 4.24 Å. Therefore, the XRD results are more accurate and repeatable, with less error compared with macroscopic curvature measurements. More importantly, the XRD method is capable of providing stress gradient information through the film thickness, which is not attainable by the curvature method. The focus of this paper is to accurately and reliably characterize residual stress in TiN thin films with different thickness using XRD.

2. Experimental procedure and theoretical analysis

2.1. TiN films deposition

TiN thin films were deposited by reactive radio frequency (RF) pulsed magnetron sputtering using a custom-built physical vapor deposition (PVD) system at 300 °C on 500 μm thick (100) Si single crystal substrates. Prior to placing them into the sputtering chamber, substrates were cleaned in acetone for 10 min and then ethanol for 10 min using an ultrasonic bath cleaner. Before sputtering, Ar^+ ion bombardment at 100 W was employed for 20 min to remove impurities and activate the surface.

The vacuum chamber was heated to 300 °C and the base pressure was better than 4.5×10^{-3} Pa. During deposition, the target power was 300 W. Meanwhile, nitrogen and argon flow was 1.2 and 30 sccm, respectively. In the sputtering chamber, the deposition pressure was kept at 2.7×10^{-1} Pa. Prior to sputtering, the target was cleaned by argon gas (Ar) discharge plasma for 5 min. To improve TiN film adhesion, Ti interlayer was deposited using Ti target with 76 mm diameter. The purity of the metallic Ti target, nitrogen gas (N_2) and Ar used was 99.995%, 99.99% and 99.99%, respectively. The target-to-substrate distance was 70 mm. The rotation rate of the sample holder was 15 rpm. After deposition, thin films were cooled to room temperature in the vacuum chamber for 3 h.

2.2. TiN films characterization

Field emission scanning electron microscopy (FESEM, Zeiss Supra™ 55) with 20 kV accelerating voltage was employed to characterize the film thickness, microstructure, surface and cross-section morphology. TiN thin film Young's modulus was measured by nanoindentation with Berkovich diamond indenter tip using Hysitron TI 900 TriboIndenter. X-ray diffractometer (Cu $K_{\alpha 1}$ radiation, λ = 1.5406 Å, Rigaku SmartLab 9 kW) was employed for crystallographic structure examination and residual stress measurements.

2.3. Stress measurement and analysis

X-ray diffractometer equipped with thin film accessory and in-house designed optimized sample stage, was employed to measure thin film residual stress in this study. Parallel beam and grazing incidence diffraction geometries were used. The side-inclination method was used to measure residual stress in TiN films. X-ray diffraction 2 theta scans were obtained and the grazing incidence X-ray diffractometry (GIXRD) was utilized in the measurements. The advantages of GIXRD include limiting the beam penetration depth into the sample, enhancing the signal from the thin film and eliminating substrate diffraction at the same time.

Fig. 1 shows XRD patterns of the 2.9 μm TiN thin film on silicon substrate obtained using both the Bragg-Brentano and the grazing incidence parallel beam optics. While regular 2 theta scan in Fig. 1(a) has higher intensity with very strong (100) Si diffraction peak, the grazing incidence parallel beam optics provides more information about the film rather than the substrate in Fig. 1(b). XRD pattern in Fig. 1(b) indicates (111) preferred orientation of the 2.9 μm TiN thin film.

In this study, residual stress of the thin film was calculated based on a modified $\sin^2\psi$ method (the so-called $\cos^2\alpha\ \sin^2\psi$ method), which utilizes asymmetric diffraction geometry. This method has the same basic principles as the traditional $\sin^2\psi$ method. Thin film biaxial residual stress is determined by measuring the lattice spacing d_{hkl} at varying inclination angle ψ. It is worth pointing out that in a single measurement, fixed (hkl) Bragg reflection plane is selected. The bi-axial strain in the $\cos^2\alpha\ \sin^2\psi$ method is given by [35]:

$$\frac{d_{\alpha\psi} - d_0}{d_0} = \frac{1+\nu}{E}\sigma\cos^2\alpha\sin^2\psi + \frac{1+\nu}{E}\sigma\sin^2\alpha - \frac{2\nu}{E}\sigma \quad (1)$$

Here, $d_{\alpha\psi}$ and d_0 represent the lattice spacing obtained from the (hkl) planes and lattice spacing of the stress-free sample, respectively. It is assumed that the material is isotropic, and consequently, Young's modulus $E_{hkl} = E$, and the Poisson ratio $\nu_{hkl} = \nu$. The slope of the linear fitting results between the strain $\frac{d_{\alpha\psi} - d_0}{d_0}$ and $\cos^2\alpha\ \sin^2\psi$ is $\frac{1+\nu}{E}\sigma$, so residual stress is obtained from the measured strain based on the Hooke's law. Fig. 2 shows schematic diagram of the grazing incidence X-ray diffractometry, and the instrumental angles are as follows. θ is the Bragg's angle, γ is the grazing incidence angle, α is the angle between the sample surface and the diffraction plane, and ψ is the inclination angle of the sample surface. Apparently, $\alpha = \theta - \gamma$, where θ is the Bragg's angle of the (hkl) planes. Combining parallel beam coming from the multi-layer mirror with a long parallel slit analyzer (PSA) yields accurate high resolution data not affected by the sample shape [36]. In brief, parallel beam optics, grazing incidence diffraction geometry and side-inclination method are adopted for appropriate penetration depth into the sample, increasing the diffraction volume in thin films and reducing the system error.

In current study, TiN (220) diffraction plane peak (2θ = 61.812°) was selected to determine biaxial stress in all measurements. The grazing incidence angle was fixed at 3°, while eight different inclination angles were ranging from 0° to 45° (0, 15°, 20°, 25°, 30°, 35°, 40° and 45°). Parameters relevant to X-ray residual stress measurements are

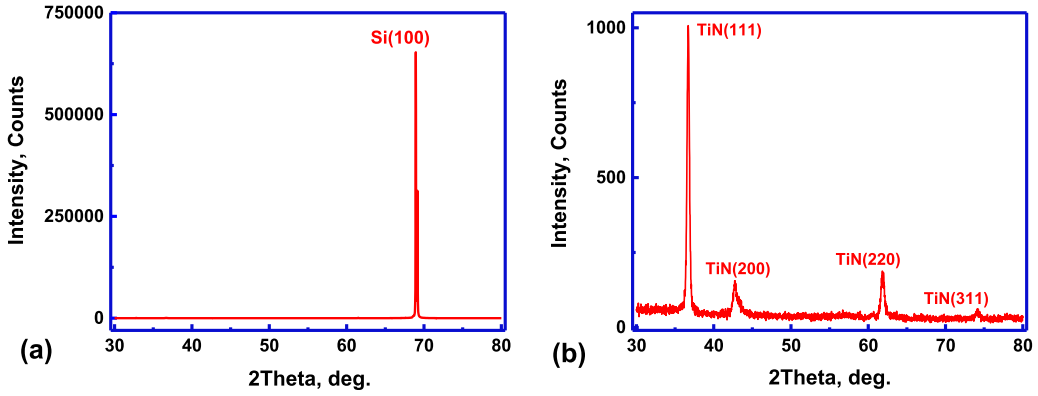

Fig. 1. X-ray diffraction patterns of 2.9 μm TiN thin film on silicon substrate obtained using (a) regular Bragg-Brentano beam optics and (b) grazing incident parallel beam optics.

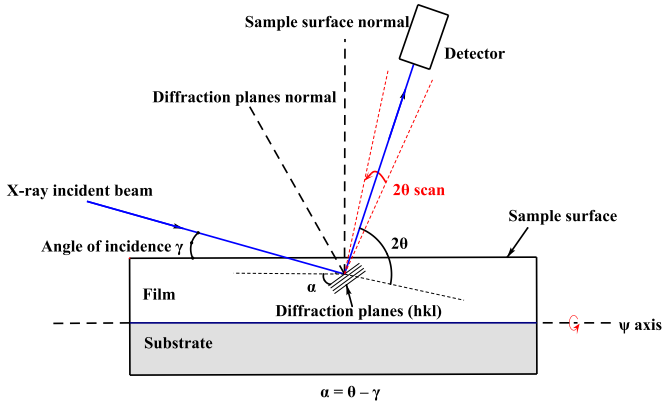

Fig. 2. Schematic diagram of grazing incidence X-ray diffractometry (GIXRD).

Table 1
Parameters used in residual stress measurements by XRD.

Material	TiN (JCPDS#38-1420)
Wavelength, λ	Cu $K_{\alpha 1}$ (1.5406 Å)
Linear absorption coefficient, μ	879 cm^{-1}
Reflection planes, (*hkl*)	(220)
Diffraction angle, 2θ	61.812°
Young's modulus, E	232.6 GPa
Poisson ratio, ν	0.21
Lattice spacing, d_0	1.4997 Å

listed in Table 1.

3. Results and discussion

3.1. Film structure

Morphology and thickness of the sputtered thin films was characterized by SEM. TiN film cross-section morphology is shown in Fig. 3, where the film is homogeneous and dense. Average surface roughness, measured by an optical profiler (White Light Interferometry, Bruker), was approximately 5.6 nm. Fig. 3 shows cross-section morphology of the TiN films with about 2 μm thickness. TiN film has a dense and columnar structure. The film thickness ranged from 1 to 3 μm (0.9, 1.4, 2, 2.3, and 2.9 μm). In Fig. 4, XRD pattern of the 0.9 μm TiN thin film is presented. TiN peak positions are indicated, according to the JCPDS card no. 38-1420. The XRD pattern clearly indicates (200) preferred orientation of the 0.9 μm TiN thin film.

It should be pointed out that high angle 2 theta reflections are commonly preferred due to their high strain sensitivity. However, for the highly textured films, large 2 theta angle reflections usually have irregular shapes and much lower intensity, which may lead to

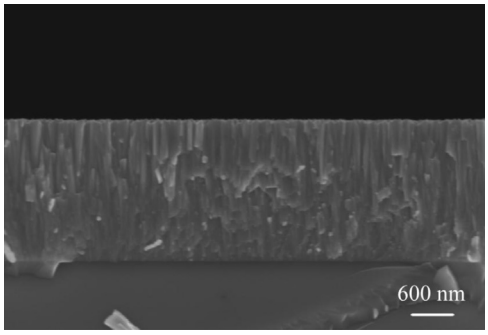

Fig. 3. SEM cross-section micrograph of 2 μm TiN film.

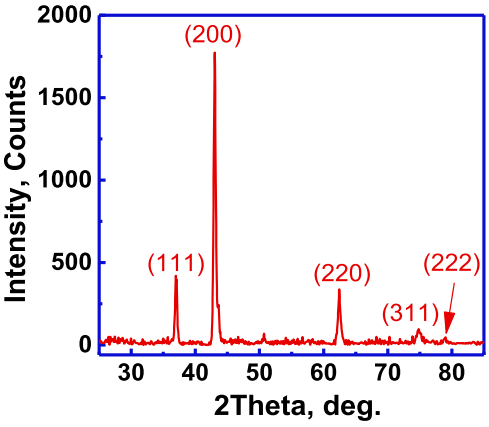

Fig. 4. X-ray diffraction pattern of the 0.9 μm TiN film obtained with grazing incidence optics.

inaccuracy when determining the peak position as well as stress calculations [35,37]. Therefore, the (220) reflection was chosen in the intermediate 2 theta range, providing low variation in the peak shape and sufficient intensity for detecting its exact position.

Table 2 shows the peak information from the GIXRD results of the TiN films with the full width at half maximum (FWHM, *B*) and grain size of TiN films (200) reflections. The grain size (*D*) was determined by the Scherrer equation [38]. Fig. 5 shows the relationship between the FWHM and the grain size with the film thickness. It can be seen that the FWHM decreased in nearly a linear way as the film thickness increased. Meanwhile, the grain size became larger, increasing from 17.51 nm (0.9 μm) to 43.06 nm (2.9 μm), and grain boundary density was reduced.

3.2. TiN films mechanical properties

Young's modulus is the key property for calculating residual stress of thin films, according to Eq. (1), which affects residual stress

Table 2
FWHM and grain size of TiN films (200) reflections.

Film thickness t (μm)	FWHM B (deg)	Grain size D (nm)
0.9	0.55	17.51
1.4	0.49	19.38
2.0	0.44	24.29
2.3	0.35	34.66
2.9	0.25	43.06

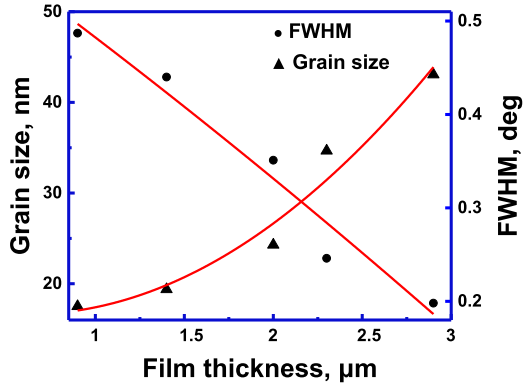

Fig. 5. FWHM and grain size of TiN (200) reflections with film thickness.

measurement accuracy. In this work, Young's modulus of thin films was measured by nanoindentation. The indenter tip was loaded at a constant rate of 200 μN/s, reaching the maximum load of 3 mN [39]. The values obtained from TiN thin films with different thickness are presented in Fig. 6. Young's modulus value were 233, 241, 226, 235, 228 and 241 GPa, respectively. Each value is an average of five indentation tests. Since the obtained modulus values are very close, an average Young's modulus value of 233 GPa was used to simplify calculation procedure.

3.3. Stress evolution with film thickness

Results of a typical residual stress measurement using TiN (220) under different inclination grazing incident parallel beam optics with the side-inclination method and the corresponding linear fitting are shown in Fig. 7 for the 2.9 μm thick film. According to the XRD peak search report, the FWHM values of the eight peaks under different inclination angles are 0.498, 0.509, 0.493, 0.494, 0.486, 0.475, 0.48 and 0.48 respectively. The averaged FWHM value is 0.498, which indicates that the TiN thin film has good crystallinity. In Fig. 6(a), all peaks have symmetric shape with relatively high intensity, while an

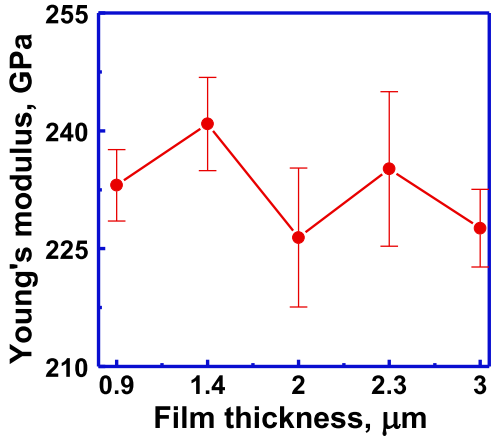

Fig. 6. Young's modulus of TiN thin films with different thickness.

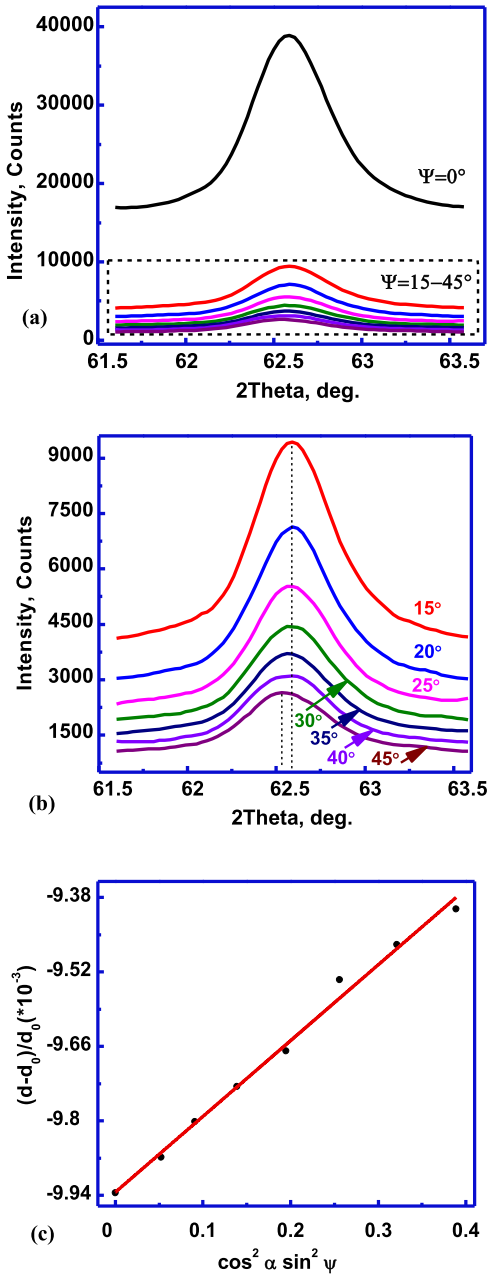

Fig. 7. (a) *Theta*-2*Theta* scans for 2.9 μm TiN film (220) reflection at different inclination angle ψ, including no inclination (ψ = 0°); (b) ψ = 15–45°; (c) corresponding $\cos^2\alpha \sin^2\psi$ plot with linear fit.

obvious peak shift is seen at different inclination angles. For better demonstration, inclined curves are shown in Fig. 6(b). Good linear fit in Fig. 6(c) indicates that the calculated residual stress values are reliable. Given the narrow 2 theta scan range (61.5–64°), the method of residual stress measurement used in this study is effective and reliable.

Table 3 shows the residual stress and Young's modulus for TiN films. Stress evolution with film thickness is also illustrated in Fig. 8. For thin films with less than 2 μm thickness, compressive residual stress is present. The thinnest 0.9 μm film has the highest compressive stress of −2 GPa. Compressive residual stress decreased to −1.4 GPa when the film thickness was 1.4 μm. When the film thickness was about 2 μm, the compressive-to-tensile transition of residual stress was observed. Tensile stress of 0.19 GPa was observed in 2 μm TiN film, while residual stress continued to increase slightly with the film thickness. TiN films with 2.3 μm and 2.9 μm thickness have tensile residual stress of 0.21 GPa and 0.28 GPa, respectively.

Table 3
Residual stress and Young's modulus of TiN films.

Film thickness t (μm)	Residual stress σ (GPa)	Young's modulus E (GPa)
0.9	−2.01	240.86
1.4	−1.40	226.42
2.0	0.19	235.15
2.3	0.21	227.6
2.9	0.28	240.9

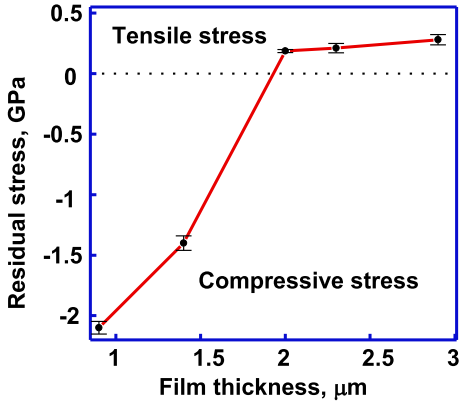

Fig. 8. Residual stress evolves with TiN film thickness.

The reasons for the residual stress sign transition phenomenon may be as follows. First, the residual stress may have changed during the film growth. At the early stage of film growth, atomic peening is the dominant mechanism. In the films with relatively small thickness, large compressive stresses are considered to be caused by the atomic peening effect. However, the peening mechanism is not strong enough to consistently generate large compressive residual stress [40–42].

When the film growth proceeds to a certain stage, the dominating mechanism will switch to recovery. Film deposition is a non-equilibrium process. Different thin film residual stress is a result of different microstructure formed. There is not enough time for surface atoms to diffuse during deposition, causing the formation of metastable structures. After deposition, the metastable structure can undergo spontaneous phase transformations and ordering, recover to a more stable state with lower energy. During this recovery process, the ordering of atoms and annihilation of cavities and defects will lead to volume shrinkage and densification of thin films. Consequently, tensile residual stresses arise in thin films. Thicker films will have more cavities and defects. As a result, when the film reaches a specific thickness, recovery takes the leading position over atomic peening.

Second, the stress transition is closely correlated with the growth mechanism of sputtered thin films. It can be seen from the comparison of Figs. 1(b) and 4 that the transition of grain size and preferred orientation comes along with the compressive-to-tensile stress transition. When TiN film thickness is relatively small, grain size is also small and the film preferred orientation is (200), which is not the close-packed plane [43]. Grain size increases with the film thickness, and (111) becomes the preferred orientation, which is the close-packed plane. The most close-packed planes are known to have the lowest surface energy. At the same time, they are the slow growth planes, which survive at the expense of fast growth planes [44].

Lower grain boundaries density has less possibility to insert extra atoms into the grain boundaries, so compressive stress decreases and gradually transforms to tensile [34]. In other words, compressive-to-tensile transition phenomenon is attributed to both the crystal densification effect and the effect of competitive grains growth with different orientation [19,45].

4. Conclusions

In this study, brittle TiN thin films with the thickness ranging from 1 to 3 μm were prepared by reactive RF-pulsed magnetron sputtering. The residual stresses in films were investigated by X-ray diffraction. The accuracy and reliability were ensured by applying the $\cos^2\alpha \sin^2\psi$ method with certain optimization, namely grazing incident parallel beam optics and side-inclination geometry.

Thickness-dependent residual stress compressive-to-tensile transition in sputtered TiN films was observed. The magnitude of compressive stress is larger than tensile stress. Highest compressive residual stress of −2 GPa was present in the 0.9 μm thick film and stress decreased with film thickness. Meanwhile, tensile stress of less than 0.3 GPa was present in 2 μm TiN films. The critical thickness for the compressive-to-tensile stress transition was approximately 2 μm. The grain size became larger with film thickness, and consequently the grain boundary density became lower. The preferred orientation changed from (200) to (111) with film thickness, along with the residual stress sign transition. Microstructure change with growth, annihilation of grain boudaries, mechanism transition from atomic peening to recovery are responsible for the reported stress sign transition.

Acknowledgements

This work was supported by the the National Key Research and Development Program of China (No. 2016YFB0700201). And the Beijing Nova Program (Z171100001117075). The author would like to thank Haijiao Xie from Shiyanjia lab for the support of SEM analysis. AV acknowledges support from the National Science Foundation (IRES 1358088).

References

[1] D. Dinesh Kumar, N. Kumar, S. Kalaiselvam, S. Dash, R. Jayavel, Substrate effect on wear resistant transition metal nitride hard coatings: microstructure and tribo-mechanical properties, Ceram. Int. 41 (2015) 9849–9861.
[2] D. Escobar, R. Ospina, A.G. Gómez, E. Restrepo-parra, Microstructure, residual stress and hardness study of nanocrystalline titanium – zirconium nitride thin films, Ceram. Int. 41 (2015) 947–952.
[3] R. Machunze, G.C.A.M. Janssen, Stress gradients in titanium nitride thin films, Surf. Coat. Technol. 203 (2008) 550–553.
[4] N.G. Ferreira, E. Abramof, N.F. Leite, E.J. Corat, V.J. Trava-Airoldi, Analysis of residual stress in diamond films by X-ray diffraction and micro-Raman spectroscopy, J. Appl. Phys. 91 (2002) 2466–2472.
[5] O. Borrero-Lopez, M. Hoffman, Measurement of fracture strength in brittle thin films, Surf. Coat. Technol. 254 (2014) 1–10.
[6] F. Lomello, M.A. Pour, F. Sanchette, F. Schuster, M. Tabarant, A. Billard, Temperature dependence of the residual stresses and mechanical properties in TiN/CrN nanolayered coatings processed by cathodic arc deposition, Surf. Coat. Technol. 238 (2014) 216–222.
[7] V. Teixeira, Residual stress and cracking in thin PVD coatings, Vacuum 64 (2002) 393–399.
[8] W.P. Vellinga, M. Van den Bosch, M.G.D. Geers, Interaction between cracking, delamination and buckling in brittle elastic thin films, Int. J. Fract. 154 (2008) 195–209.
[9] T. Guo, L. Qiao, X. Pang, A.A. Volinsky, Brittle film-induced cracking of ductile substrates, Acta Mater. 99 (2015) 273–280.
[10] V. Teixeira, Mechanical integrity in PVD coatings due to the presence of residual stresses, Thin Solid Films 392 (2001) 276–281.
[11] J.F. Chang, C.C. Shen, M.H. Hon, Growth Characteristics and Residual Stress of RF Magnetron Sputtered ZnO: Al Films, vol. 29, 2003, pp. 245–250.
[12] G. Liu, Y. Yang, B. Huang, X. Luo, S. Ouyang, G. Zhao, et al., Effects of substrate temperature on the structure, residual stress and nanohardness of Ti6Al4V films prepared by magnetron sputtering, Appl. Surf. Sci. 370 (2016) 53–58.
[13] A. Al-masha, A. Bunting, R. Cheung, Evaluation of residual stress in sputtered tantalum thin-film, Appl. Surf. Sci. 371 (2016) 571–575.
[14] R. Machunze, G.C.a.M. Janssen, Stress and strain in titanium nitride thin films, Thin Solid Films 517 (2009) 5888–5893.
[15] H. Köstenbauer, G.a. Fontalvo, M. Kapp, J. Keckes, C. Mitterer, Annealing of intrinsic stresses in sputtered TiN films: the role of thickness-dependent gradients of point defect density, Surf. Coat. Technol. 201 (2007) 4777–4780.
[16] E. Dobroˇ, P. Novák, D. Búc, L. Harmatha, J. Murín, X-ray diffraction analysis of residual stresses in textured ZnO thin films, Appl. Surf. Sci. 395 (2017) 16–23.
[17] D. Biswas, A. Kumar, S. Chakraborty, Effects of oxygen partial pressure and annealing temperature on the residual stress of hafnium oxide thin-films on silicon using synchrotron-based grazing incidence X-ray diffraction, Appl. Surf. Sci. 384 (2016) 376–379.

[18] A. Wang, C. Chuang, G. Yu, J. Huang, Determination of average X-ray strain (AXS) on TiN hard coatings using $\cos^2\alpha\sin^2\psi$ X-ray diffraction method, Surf. Coat. Technol. 262 (2015) 40–47.
[19] R. Daniel, K.J. Martinschitz, J. Keckes, C. Mitterer, The origin of stresses in magnetron-sputtered thin films with zone T structures, Acta Mater. 58 (2010) 2621–2633.
[20] W.J. Chou, G.P. Yu, J.H. Huang, Mechanical properties of TiN thin film coatings on 304 stainless steel substrates, Surf. Coat. Technol. 149 (2002) 7–13.
[21] C.L. Chang, J.Y. Jao, W.Y. Ho, D.Y. Wang, Influence of bi-layer period thickness on the residual stress, mechanical and tribological properties of nanolayered TiAlN/CrN multi-layer coatings, Vacuum 81 (2007) 604–609.
[22] L. Karlsson, A. Hörling, M. Johansson, The influence of thermal annealing on residual stresses and mechanical properties of arc-evaporated TiC_xN_{1-x} (x = 0, 0.15 and 0.45), Acta Mater. 371 (2002) 5103–5114.
[23] D.C. Tsai, Z.C. Chang, B.H. Kuo, Y.S. Deng, E.C. Chen, F.S. Shieu, Effects of sputtering power on microstructure and mechanical properties of TiVCr films, Vacuum 125 (2016) 227–233.
[24] W. Tillmann, T. Sprute, F. Hoffmann, Y.Y. Chang, C.Y. Tsai, Influence of bias voltage on residual stresses and tribological properties of TiAlVN-coatings at elevated temperatures, Surf. Coat. Technol. 231 (2013) 122–125.
[25] H. Liu, Q. Xu, X. Zhang, C. Wang, B. Tang, Residual stress analysis of TiN film fabricated by plasma immersion ion implantation and deposition process, Nucl. Instrum. Methods Phys. Res. Sect. B Beam Interact. Mater. At. 297 (2013) 1–6.
[26] R. Treml, D. Kozic, J. Zechner, X. Maeder, B. Sartory, H.-P. Gänser, et al., High resolution determination of local residual stress gradients in single- and multilayer thin film systems, Acta Mater. 103 (2016) 616–623.
[27] M. Wittmer, B. Studer, H. Melchior, Electrical characteristics of TiN contacts to N silicon, J. Appl. Phys. 52 (1981) 5722–5726.
[28] H. Uchida, S. Inoue, K. Koterazawa, Electrochemical evaluation of pinhole defects in TiN films prepared by r.f. reactive sputtering, Mater. Sci. Eng. A 234–236 (1997) 649–652.
[29] F. Cai, M. Chen, M. Li, S. Zhang, Influence of negative bias voltage on microstructure and property of Al-Ti-N films deposited by multi-arc ion plating, Ceram. Int. 43 (2017) 3774–3783.
[30] K. Fu, L. Chang, B. Zheng, Y. Tang, Y. Yin, Analysis on cracking in hard thin films on a soft substrate under Berkovich indentation, Vacuum 112 (2014) 29–32.
[31] M. Stefenelli, R. Daniel, W. Ecker, D. Kiener, J. Todt, A. Zeilinger, et al., X-ray nanodiffraction reveals stress distribution across an indented multilayered CrN-Cr thin film, Acta Mater. 85 (2015) 24–31.
[32] E.A. Flores-Johnson, L. Shen, R.K. Annabattula, P.R. Onck, Y.G. Shen, Z. Chen, The effect of interface adhesion on buckling and cracking of hard thin films, Appl. Phys. Lett. 105 (2014).
[33] Y.X. Ou, J. Lin, S. Tong, H.L. Che, W.D. Sproul, M.K. Lei, Wear and corrosion resistance of CrN/TiN superlattice coatings deposited by a combined deep oscillation magnetron sputtering and pulsed dc magnetron sputtering, Appl. Surf. Sci. 351 (2015) 332–343.
[34] L. Zhang, H. Yang, X. Pang, K. Gao, A.a. Volinsky, Microstructure, residual stress, and fracture of sputtered TiN films, Surf. Coat. Technol. 224 (2013) 120–125.
[35] C.H. Ma, J.H. Huang, H. Chen, Residual stress measurement in textured thin film by grazing-incidence X-ray diffraction, Thin Solid Films 418 (2002) 73–78.
[36] A. Nezu, H. Matsuzaka, R. Yokoyama, A current perspective of the state-of-the-art in stress analysis, Rigaku J. 30 (2014) 4–12.
[37] A.N. Wang, J.H. Huang, H.W. Hsiao, G.P. Yu, H. Chen, Residual stress measurement on TiN thin films by combing nanoindentation and average X-ray strain (AXS) method, Surf. Coat. Technol. 280 (2015) 43–49.
[38] K. Kusaka, T. Ao, T. Hanabusa, K. Tominaga, Effect of external magnetic field on c-axis orientation and residual stress in AlN films, Thin Solid Films 332 (1998) 247–251.
[39] Xiao Chen, Yeting Xi, Jie Meng, Xiaolu Pang, Huisheng Yang, Effects of substrate bias voltage on mechanical properties and tribological behaviors of RF sputtered multilayer TiN/CrAlN films, J. Alloy. Compd. 665 (2016) 210–217.
[40] T. Sasabayashi, N. Ito, E. Nishimura, M. Kon, P.K. Song, K. Utsumi, et al., Comparative study on structure and internal stress in tin-doped indium oxide and indium-zinc oxide films deposited by r.f. magnetron sputtering, Thin Solid Films 445 (2003) 219–223.
[41] K. Kusaka, D. Taniguchi, T. Hanabusa, K. Tominaga, Effect of sputtering gas pressure and nitrogen concentration on crystal orientation and residual stress in sputtered AlN films, Vacuum 66 (2002) 441–446.
[42] H. Windischmann, An intrinsic stress scaling law for polycrystalline thin films prepared by ion beam sputtering, J. Appl. Phys. 62 (1987) 1800–1807.
[43] S.K. Wu, H.C. Lin, P.L. Liu, An investigation of unbalanced-magnetron sputtered TiAlN films on SKH51 high-speed steel, Surf. Coat. Technol. 124 (2000) 97–103.
[44] C.T. Chen, Y.C. Song, G.-P. Yu, J.-H. Huang, Microstructure and hardness of hollow cathode discharge ion-plated titanium nitride film, J. Mater. Eng. Perform. 7 (1998) 324–328.
[45] P. Chaudhari, Grain growth and stress relief in thin films, J. Vac. Sci. Technol. 9 (1972) 520.